Highly Efficient Red Phosphorescent OLEDs based on Non-Conjugated Silicon-Cored Spirobifluorene Derivative Doped with Ir-Complexes

ARTICLE *in* ADVANCED FUNCTIONAL MATERIALS · FEBRUARY 2009

Impact Factor: 11.81 · DOI: 10.1002/adfm.200801319

8 AUTHORS, INCLUDING:

Jeonghun Kwak
University of Seoul
63 PUBLICATIONS **988** CITATIONS
SEE PROFILE

Younghun Byun
Samsung Advanced Institute of Technology
21 PUBLICATIONS **435** CITATIONS
SEE PROFILE

Doseok Kim
Sogang University
122 PUBLICATIONS **2,129** CITATIONS
SEE PROFILE

Changhee Lee
Seoul National University
293 PUBLICATIONS **4,089** CITATIONS
SEE PROFILE

FULL PAPER

Highly Efficient Red Phosphorescent OLEDs based on Non-Conjugated Silicon-Cored Spirobifluorene Derivative Doped with Ir-Complexes

By *Yi-Yeol Lyu, Jeonghun Kwak, Woo Sung Jeon, Younghun Byun, Hyo Sug Lee, Doseok Kim, Changhee Lee,** and *Kookheon Char**

A novel host material containing silicon-cored spirobifluorene derivative (SBP-TS-PSB), is designed, synthesized, and characterized for red phosphorescent organic light-emitting diodes (OLEDs). The SBP-TS-PSB has excellent thermal and morphological stabilities and exhibits high electroluminescence (EL) efficiency as a host for the red phosphorescent OLEDs. The electrophosphorescence properties of the devices using SBP-TS-PSB as the host and red phosphorescent iridium (III) complexes as the emitter are investigated and these devices exhibit higher EL performances compared with the reference devices with 4,4′-*N*,*N*′-dicarbazole-biphenyl (CBP) as a host material; for example, a $(piq)_2Ir(acac)$-doped SBP-TS-PSB device shows maximum external quantum efficiency of $\eta_{ext} = 14.6\%$, power efficiency of 10.3 lm W^{-1} and Commission International de L'Eclairage color coordinates (0.68, 0.32) at $J = 1.5$ mA cm^{-2}, while the device with the CBP host shows maximum $\eta_{ext} = 12.1\%$. These high performances can be mainly explained by efficient triplet energy transfer from the host to the guests and improved charge balance attributable to the bipolar characteristics of the spirobifluorene group.

1. Introduction

Organic light-emitting diodes (OLEDs) have been intensively investigated for their applications in high-efficiency, low-drive voltage, full-color, large-area flat-panel displays.[1] Phosphorescent OLEDs are of great interest because it is possible, in principle, to increase the internal quantum efficiency to 100%, corresponding to an external quantum efficiency more than 20%.[2] These devices use emissive layers comprising a conductive host doped with a phosphorescent heavy metal complexes emitting from the triplet metal-to-ligand charge transfer (^{3}MLCT) state. As the triplet and singlet MLCT states are mixed intimately in these complexes, light can be harvested from both the singlet and triplet excitons. Since conventional red fluorescent emitters are not as good as green or blue fluorescent emitters, much research is focused on achieving higher efficiency from red phosphorescent devices.[3–5] The efforts are concentrated on getting the improved red phosphorescent emitters with higher efficiency and color purity. For the most part, 4,4′-*N*,*N*′-dicarbazole-biphenyl (CBP) has been used as the host material for red phosphorescent emitters since it exhibits ambipolar conduction when doped with phosphorescent dopants[2f] and its high triplet energy ($E_T \approx 2.55$ eV)[2g] allows exothermic energy transfer conditions for red and green phosphorescent emitters.[2d,3,5a,c,d] The red emitting complexes $(btp)_2Ir(acac)$ [2d,e] (btp = 2-(2′-benzo[4,5-α]thienyl)pyridinato), $(piq)_3Ir$[3] (piq = 1-phenylisoquinolinato), and $(piq)_2Ir(acac)$[4] (acac = acethylaceotonate), when doped into CBP, show external quantum efficiencies (η_{ext}) of 7.0% at 0.1 mA cm^{-2}, 10.3% at 100 cd m^{-2}, and 9.21% at 100 mA cm^{-2}, respectively. The choice of a correct host material is very challenging as the host should have i) a large band gap for the exothermic energy transfer from the host to the dopant, ii) high glass transition temperature (T_g) for a durable devices, and iii) balanced charge carrier transport for the electron–hole (e–h) recombination process and confinement of the exciton formation zone in the emissive layer. These attributes of the host materials are very important in determining the device performance. There have been some reports of using hosts other than CBP in the red phosphorescent OLEDs to obtain higher device performance. Non-conjugated hybrids of carbazole-fluorene[6] and spiro-configured bifluorene[7] are used as the host materials for red phosphorescent emitters due to their bipolar characteristics and high thermal stabilities.

[*] Prof. C. H. Lee, J. Kwak
School of Electrical Engineering and Computer Science
Inter-University Semiconductor Research Center
Seoul National University
599 Gwanakro, Gwanak-ku, Seoul 151-742 (Korea)
E-mail: chlee7@snu.ac.kr
Prof. K. Char
School of Chemical and Biological Engineering
NANO Systems Institute-National Core Research Center
Seoul National University
599 Gwanakro, Gwanak-ku, Seoul 151-742 (Korea)
E-mail: khchar@plaza.snu.ac.kr
Dr. Y.-Y. Lyu, Dr. W. S. Jeon, Dr. Y. Byun, Dr. H. S. Lee
Samsung Advanced Institute of Technology, Mt. 14-1, Nongseo-Ri
Giheung-Eup, Yongin-Si, Gyeonggi-Do 449-712 (Korea)
Prof. D.-S. Kim
Department of Physics, Sogang University
1 Sinsoo, Mapo-gu, Seoul 100-611 (Korea)

DOI: 10.1002/adfm.200801319

In this study, we report highly efficient phosphorescent OLEDs using a non conjugated silicon-cored spirobifluorene derivative (**SBP-TS-PSB**) as a host material for the red phosphorescent Ir(III) complexes. While designing the host, we gave emphasis on i) the high thermal and morphological stabilities, ii) prevention of concentration quenching, and iii) increase in flexibility. For that we connected spirobifluorene derivatives at the *meta*-positions of two phenyl groups with tetraphenylsilane as a core material, as shown in Figure 1, to obtain a sterically hindered twisted structure for the prevention of concentration quenching and the enhancement of morphological stability. Additionally, we introduced the aryl groups at C2 position of spirobifluorene units in order to obtain the proper conjugation necessary for a host material. Since the π-conjugation length and the mode of interconnection determines the highest occupied molecular orbital (HOMO), lowest unoccupied molecular orbital (LUMO), and triplet energy levels and consequently the charge injection, transport, and exciton transfer to the dopant, a proper molecular design is most helpful in achieving the best device performance. In this regard **SBP-TS-PSB** is expected to be an excellent host for the red emitting phosphorescent OLEDs.

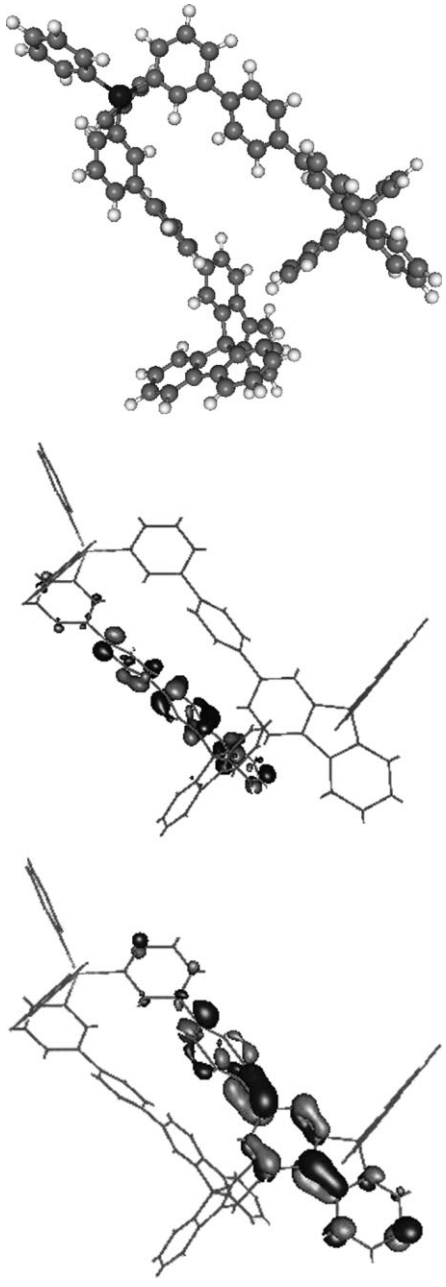

Figure 1. Optimized geometries and calculated highest occupied molecular orbital (HOMO) and lowest unoccupied molecular orbital (LUMO) density maps of **SBP-TS-PSB**.

The presence of spirobifluorene units can make the molecule ambipolar and enable the transport of both electrons and holes for the efficient exciton formation and confinement away from both the hole-transporting layer (HTL) and the electron-transporting layer (ETL). This tetraphenylsilane-cored spirobifluorene derivative host material shows high thermal stability and substantial amorphous thin film forming capability. Three phosphorescent guests, $(piq)_3Ir$, $(piq)_2Ir(acac)$, and $(btp)_2Ir(acac)$ were doped in the **SBP-TS-PSB** host and the device performances were investigated. All of these red OLEDs exhibit higher electroluminescence (EL) efficiency compared to the devices consisting of the same guests doped in a conventional host material of CBP. For example, the $(piq)_2Ir(acac)$-doped **SBP-TS-PSB** device shows maximum external EL quantum efficiency of $\eta_{ext} = 14.6\%$ while the device with the CBP host shows maximum $\eta_{ext} = 12.1\%$.

2. Results and Discussion

2.1. Synthesis, Molecular Structure, and Characterization of SBP-TS-PSB

The chemical structure and synthetic routes of the host material **SBP-TS-PSB** are shown in Scheme 1. Compound **1** was synthesized by reacting 2-bromo-9,9′-spirobifluorene[8] with an excess of *n*-BuLi at −78 °C, followed by treating the lithiated complex with 2-isopropoxy-4,4,5,5-tetramethyl-1,3,2-dioxaborolane. Suzuki coupling reactions of 1-bromo-4-iodobenzene with compound **1**, in the presence of a catalytic amount of $Pd(PPh_3)_4$ and 2 M K_2CO_3, yielded the monobrominated compound **2**. Compound **3** was synthesized by a method analogous to that used for compound **1**. Pd-catalyzed Suzuki coupling reactions of bis (3-bromophenyl) diphenylsilane[9] with the boronate compound **3** was employed for the synthesis of **SBP-TS-PSB**. Elemental analysis (EA), ^1H NMR, ^{13}C NMR, and mass spectral data are consistent with the proposed structure.

Figure 1 shows the three-dimensional structure of **SBP-TS-PSB** optimized by theoretical calculations. The calculations were performed using the B3LYP hybrid functional and the 6-31G(d) basis sets implemented in the Gaussian-98 suite of programs.[10–12] The structure of **SBP-TS-PSB** has a tetrahedral structure in which a silicon atom is located at the center of the tetrahedron. Two of the phenyl groups bonded to the silicon atom connect at the C3 atom (*m*-position) with the C4 atom (*p*-position) of the 1-(9,9′-spirobifluorene-2-yl)benzene group. The biphenyl groups have a dihedral angle of 137.9° and the phenyl group and spirobifluorene group are twisted to angles 139.3°. From this calculation the **SBP-TS-PSB** has a non-coplanar structure and disrupts the

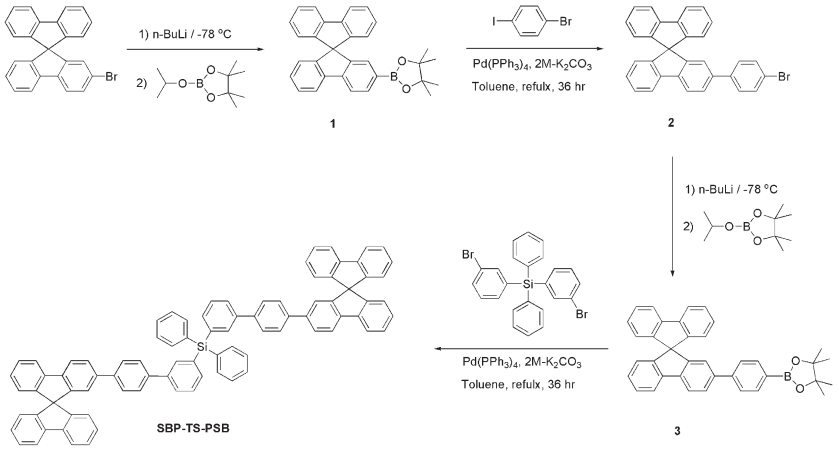

Scheme 1. Synthetic routes to **SBP-TS-PSB**. Details are given in Section 4.

intermolecular interactions, which improves the morphological stability of the thin film devices. In previous experimental and theoretical reports on the study of the energy levels of the hosts derived from spirofluorene, the relationship of the conjugation length of the phenyl rings in the *p*- and *m*-positions and triplet energy have been derived.[13,14] The degree of delocalization of the triplet wave function determines the triplet energy. In the present molecular structure, the two phenyl rings of spirobifluorene and the tetraphenylsilane group are interconnected at the *p*–*p*-positions of phenylene ring. But the *p*–*p*- interconnection is interrupted when the phenyl ring is bonded to silicon at the *m*-position. This would raise the triplet energy higher than all the *p*-connected four phenyl groups would do, simultaneously imparting flexibility to the molecular structure. The calculated HOMO and LUMO densities of **SBP-TS-PSB** are presented in Figure 1. The delocalized π-electrons are spread over the three phenyl rings instead of four phenyl rings and we expect this material as a suitable host for the red phosphorescent OLEDs.

Figure 2 shows the optical absorption and fluorescence spectra of **SBP-TS-PSB** in solution and film, measured at room temperature, and normalized phosphorescence spectrum of **SBP-TS-PSB** solution measured at 77 K. Both absorption (312, 329 nm) and fluorescence (363, 381 nm) peaks in solution are redshifted in the film, implying intermolecular interactions in the film. No peak in the longer wavelength region is observed, negating the possibility of any excimer emission. We presume that the quaternary silicon core serves as a spacer to effectively block the extended π-conjugation of the spirobifluorene units on both sides. The normalized phosphorescence spectrum of **SBP-TS-PSB** solution at 77 K shows a phosphorescence peak at 408 nm, corresponding to the triplet energy of 3.04 eV. It is higher than the triplet energy of red phosphorescent dopants ($E_T \approx 2.0$ eV) such as $(btp)_2Ir(acac)$, $(piq)_3Ir$, and $(piq)_2Ir(acac)$. Therefore, **SBP-TS-PSB** can be a suitable a host material for red phosphorescent emitters allowing efficient triplet energy transfer from the host to the dopant.

The redox potentials of **SBP-TS-PSB** were monitored by cyclic voltammetry. Figure 3 shows typical voltammograms of **SBP-TS-PSB** in 0.1 M nBu_4NPF_6 as supporting electrolyte, using ferrocene as the internal standard. During the anodic scan in CH_2Cl_2, **SBP-TS-PSB** exhibits a reversible oxidation process [apparent $E_{1/2}^{(OX)} = 1.04$ V (vs. Fc/Fc^+)], whereas the cathodic sweep in THF shows a quasi-reversible reduction process with apparent $E_{1/2}^{(red)} = -2.79$ V (vs Fc/Fc^+), appearing near the edge of potential window THF. From the cyclic voltammetry data, we estimated the HOMO energy level (−5.84 eV) of the **SBP-TS-PSB** with reference to the Fermi energy level of ferrocene (4.8 eV). The LUMO energy level (−2.39 eV) was calculated from the HOMO

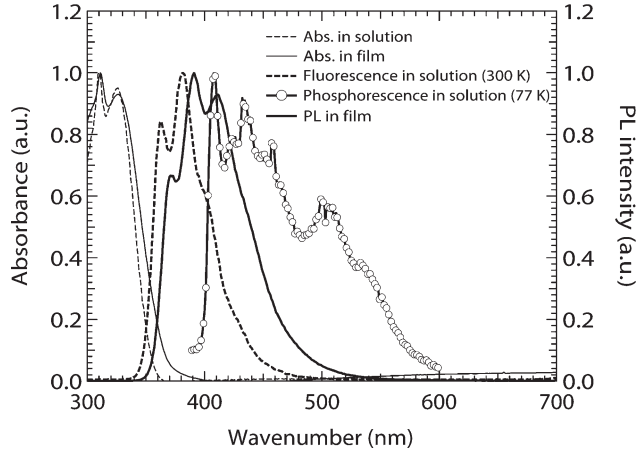

Figure 2. Normalized optical absorption and photoluminescence (fluorescence) spectra of **SBP-TS-PSB** in dilute chloroform solution (dotted line) and in solid thin films (solid line) measured at room temperature. Normalized phosphorescence spectrum (open circle) of **SBP-TS-PSB** in dilute 2-methyltetrahydrofuran solution is measured at 77 K.

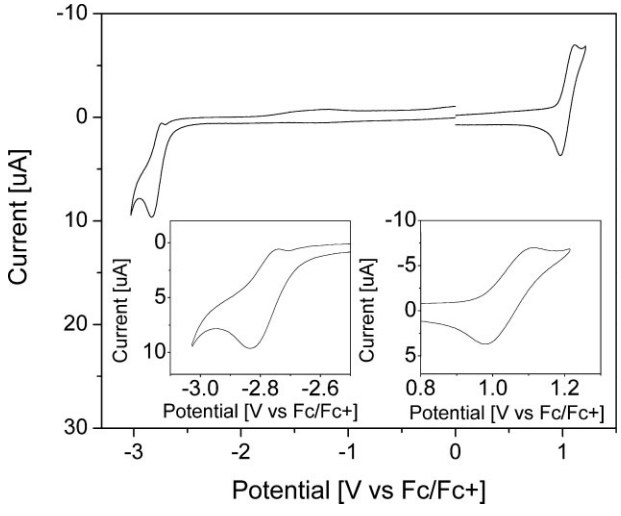

Figure 3. Cyclic voltammograms of **SBP-TS-PSB** in CH_2Cl_2 (for oxidation) or THF (for reduction) with 0.1 M Bu_4NPF_6 as a supporting electrolyte (scan rate = 200 mV s^{-1}). The insets show the reduction and oxidation potential regions in an enlarged scale.

and the lowest energy absorption of the **SBP-TS-PSB** UV–Vis absorption spectra shown in Figure 2.[15]

Figure 4 shows the differential scanning calorimetry (DSC) and thermogravimetric analysis (TGA) curves of the sublimated **SBP-TS-PSB**. The compound melted at 332 °C during the first heating cycle in the DSC measurement. The glass transition temperature was observed at 194 °C in the second, third, and forth heating scans. No crystallization temperature (T_c) was observed upon heating the sample to 450 °C and cooling to 25 °C. The compound shows the decomposition temperature (T_d; corresponding to 5% weight loss) as high as 515 °C. In comparison, CBP exhibits T_m, T_g, T_c, and T_d at 283, N. D. (not detected), 199, and 373 °C, respectively (see Figure S1 of the Supporting Information). Thus, **SBP-TS-PSB** has excellent thermal and morphological stabilities that are essential to achieve homogeneous and amorphous thin films through vacuum deposition for the stable OLEDs.

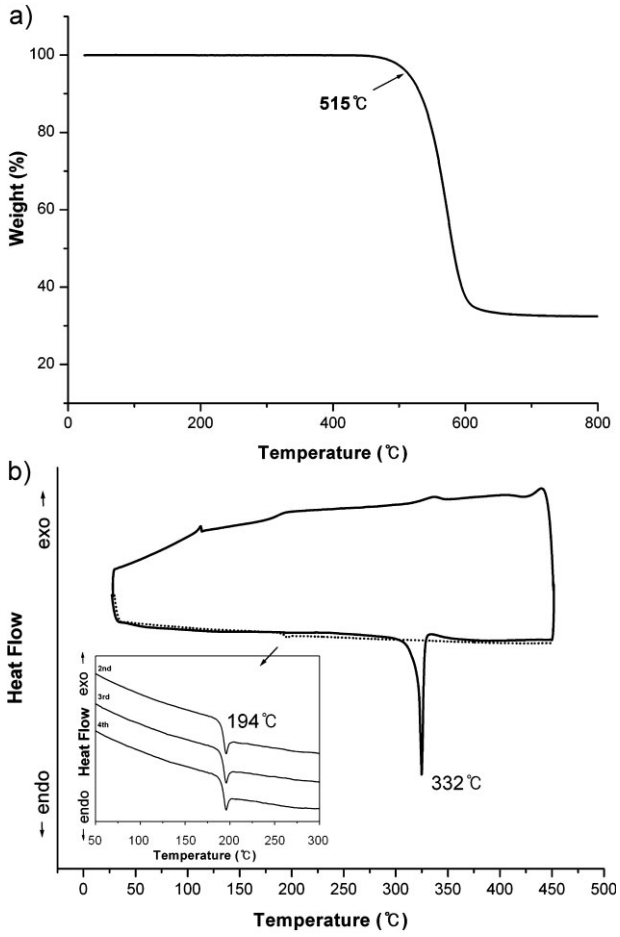

Figure 4. a) TGA thermograms of **SBP-TS-PSB**. The temperatures shown in the figure correspond to 5% weight loss. b) DSC thermograms of **SBP-TS-PSB**. The inset is the magnified view of the glass transition temperature region at 194 °C in the second, third, and forth heating scans.

2.2. Electroluminescence and Current Density–Voltage–Luminance Characteristics of Red Phosphorescent OLEDs Based on SBP-TS-PSB Doped with Ir-Complexes

To examine the applicability of **SBP-TS-PSB** as a host in red phosphorescent OLEDs, we fabricated devices with configurations of indium tin oxide (ITO)/poly(3, 4-ethyldioxythiophene) poly-(styrenesulfonate) (PEDOT:PSS) (300 Å)/α-NPD (475 Å)/TCTA (25 Å)/red-emitting layer (300 Å)/BCP (100 Å)/Alq_3 (600 Å)/LiF (5 Å)/Al (1000 Å). Figure 5 shows a schematic energy diagram and chemical structures of **SBP-TS-PSB**, CBP, and three red-phosphorescent dopants, $(piq)_3Ir$, $(piq)_2Ir(acac)$, and $(btp)_2Ir(acac)$. Three different red-emitting layers were constructed by doping phosphorescent dyes in **SBP-TS-PSB** with a concentration of 8 wt%. The dopant materials are $(piq)_2Ir(acac)$ for device **A**, $(piq)_3Ir$ for device **B**, and $(btp)_2Ir(acac)$ for device **C**. For comparison, we fabricated the reference device (device **A′**) by doping 8 wt % $(piq)_2Ir(acac)$ in a conventional CBP host. The conducting polymer PEDOT:PSS is used as a hole injection layer (HIL), 4,4′-bis[*N*-(1-naphthyl)-*N*-phenyl-amino]biphenyl (α-NPD) as a HTL and tris(8-hydroxyquinoline) aluminum (Alq_3) as an ETL. Although the triplet energy of α-NPD ($E_T \approx 2.28$ eV[2g]) is considered sufficient to confine the red-emitting triplet excitons ($E_T \approx 2.0$ eV) within the emissive layer, we found that the insertion of a thin (25 Å) interlayer of 4,4′,4″-tri(*N*-carbazolyl)triphenylamine (TCTA) with high triplet energy ($E_T \approx 2.74$ eV[2g]) at the α-NPD/EML interface results in higher efficiency (see Table 1). This implies that a sufficiently high E_T is necessary for complete exciton confinement in the emissive layer. Similarly, a thin layer (100 Å) of 2,9-dimethyl-4,7-diphenyl-1,10-phenanthroline (BCP) with $E_T \approx$ 2.46 eV[2g] was inserted at the EML/ETL interface as a hole- and exciton-blocking layer.

Figure 6 shows normalized EL spectra of all the devices measured at room temperature applying a constant current density of

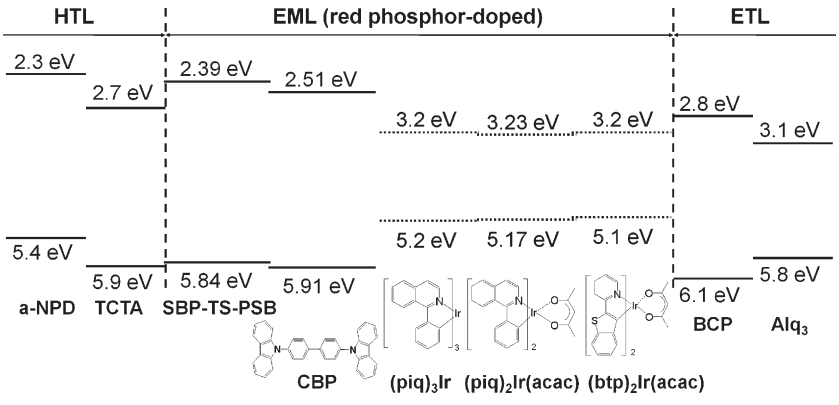

Figure 5. Schematic energy diagram of the device and chemical structures of **SBP-TS-PSB**, CBP and three red phosphorescent dopants $(piq)_3Ir$, $(piq)_2Ir(acac)$, and $(btp)_2Ir(acac)$.

Table 1. Device properties of red phosphorescent OLEDs using **SBP-TS-PSB** and common CBP hosts.

Dopant in the host of **SBP-TS-PSB**		Turn-on voltage [V]	Max brightness [cd m^{-2}]	Max quantum efficiency [%]	Max power efficiency [lm W^{-1}]	Max current efficiency [cd A^{-1}]	Color coordinates (x, y)
$(piq)_2$ Ir (acac)	**SBP-TS-PSB**w/TCTA	3.2	38 225	14.6	10.3	13.2	0.68, 0.32
	SBP-TS-PSBw/o TCTA	3.2	32 539	13.8	9.8	12.4	0.68, 0.32
	CBP host	3.4	49 313	12.1	7.0	11.5	0.68, 0.32
	$(piq)_3$Ir	3.4	26 655	13.5	7.8	12.8	0.67, 0.32
	$(btp)_2$Ir(acac)	3.2	11 446	9.9	7.0	9.7	0.66, 0.31

25 mA cm^{-2}. The photoluminescence (PL) spectra of three red dopants in the dilute chloroform solution are also plotted in Figure 6. The inset depicts the weak EL emission region around 460 nm in the 30× magnification for the $(piq)_2$Ir(acac)-doped devices with **SBP-TS-PSB** and CBP hosts. The EL spectra are identical to the PL spectra except for small redshift of 6–8 nm. In the doped devices, the EL results from either energy transfer from host to dopant or direct e-h recombination at dopant molecules. Since the HOMO and LUMO levels of the red dopants are deep inside the energy bandgap of **SBP-TS-PSB** or CBP, as shown in Figure 5, the EL from red dopants is mainly originated from direct recombination of charges trapped at the dopant molecules.[16,17] As shown in the inset of Figure 6, weak EL emission around 460 nm is more pronounced for the **SBP-TS-PSB** host with a thin TCTA interlayer, while it is almost negligible for the CBP host with the TCTA interlayer or the **SBP-TS-PSB** host without the TCTA interlayer. Therefore, it is attributed to the EL emission from TCTA and α-NPD due to the leakage of electrons from the **SBP-TS-PSB** host to TCTA/α-NPD interface and recombination with holes since the LUMO of TCTA (−2.7 eV, as shown in Fig. 5) is lower than that of **SBP-TS-PSB** (−2.39 eV). The fact that the 460-nm emission is pronounced for the **SBP-TS-PSB** host compared with the CBP host when the TCTA interlayer is inserted indicates that e–h recombination occurs near the HTL/EML interface for the **SBP-TS-PSB** host while it occurs near the EML/ETL interface for the CBP host which shows higher hole mobility.[18] This difference in the e–h recombination zone suggests that the electron conduction properties are better for **SBP-TS-PSB**, consistent with bipolar characteristics of the spirobifluorene group.

Different carrier conduction properties and energy levels (see Fig. 5) of **SBP-TS-PSB** and CBP affect the current density–voltage (*J*–*V*) characteristics and the EL efficiency vs current density (η_{ext}–*J*) as compared in Figure 7. The devices with the $(piq)_2$Ir(acac)-doped **SBP-TS-PSB** having two different HTL structures (α-NPD only and α-NPD with a thin TCTA interlayer) shows slightly lower current density at high voltage but much higher efficiency (as shown in the inset), indicating improved charge balance. As

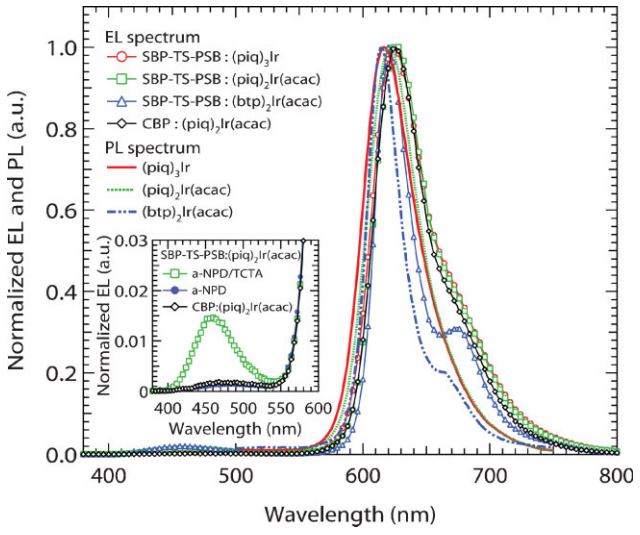

Figure 6. Normalized photoluminescence spectra of the red triplet emitters in dilute chloroform solution and EL spectra of devices employing $(piq)_3$Ir, $(piq)_2$Ir(acac), or $(btp)_2$Ir(acac) as a guest and **SBP-TS-PSB** as a host. The inset depicts the weak EL emission region around 460 nm in the 30-times magnification for the $(piq)_2$Ir(acac)-doped devices with **SBP-TS-PSB** and CBP hosts. Two different HTL structures (α-NPD only and α-NPD with a thin TCTA interlayer) are compared for the $(piq)_2$Ir(acac)-doped **SBP-TS-PSB** devices.

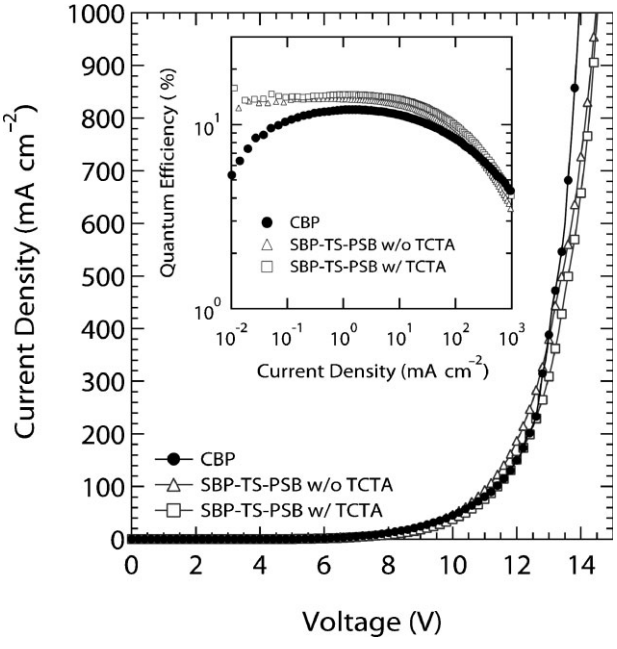

Figure 7. Current density–voltage characteristics for devices with the $(piq)_2$Ir(acac)-doped **SBP-TS-PSB** host with (square) and without (triangle) a TCTA interlayer and CBP host with the TCTA interlayer (circle). The inset shows the EL efficiency versus current density for three devices.

explained previously, for the $(piq)_2Ir(acac)$-doped **SBP-TS-PSB** device the EL efficiency is slightly higher when the TCTA interlayer is inserted at the α-NPD and the EML due to more complete exciton confinement in the EML.

The schematic energy diagram in Figure 5 suggests that the energy barrier for electron injection from the ETL is higher for **SBP-TS-PSB** compared to the CBP host but electron conduction properties are better for the doped **SBP-TS-PSB** as explained above. In both hosts, the hole transport is affected by trapping for high doping concentration of red phosphorescent molecules.[19] Therefore, the hole and electron flows are appeared to be better balanced and the e–h recombination is confined well inside EML in the $(piq)_2Ir(acac)$-doped **SBP-TS-PSB** device, leading to the high luminance efficiency. The EL efficiency for the **SBP-TS-PSB** host reaches maximum external quantum efficiency of $\eta_{ext} = 14.6\%$ at $J = 1.5\ mA\ cm^{-2}$. In the $(piq)_2Ir(acac)$-doped CBP device at low current density; however, the hole concentration in the EML exceeds electron concentration due to higher hole mobility and consequently the charge balance is not well established. As the voltage (or current) increases, the electron injection from the ETL into the EML increases and the charge balance improves, resulting in gradually increasing efficiency. After a maximum of $\eta_{ext} \approx 12.1\%$ at $J = 1.5\ mA\ cm^{-2}$ the EL efficiency slowly decreases due to the typical efficiency roll-off mechanisms.[2,20–22] The efficiency roll-off is commonly observed in phosphorescent OLEDs and several mechanisms such as triplet–triplet annihilation, exciton quenching by charge carriers, or electric-field induced dissociation of excitons were proposed.[2,20–22]

Although the devices with the **SBP-TS-PSB** host show higher efficiency, they show more rapid efficiency roll-off as the current density is increased above $10\ mA\ cm^{-2}$. This behavior can be understood as follows: as the current density increases, some electrons can move into the TCTA/α-NPD interface since electron transport can be possible in the doped **SBP-TS-PSB** host, resulting in weak EL emission around 460 nm (see the inset of Fig. 6). Thus, the e–h balance in the EML becomes worse at high current density. This additional effect, in addition to typical efficiency roll-off mechanisms, may lead to more rapid efficiency roll-off at high current density. Therefore, we expect that the EL efficiency at high current density can be improved by preventing electron leakage to the HTL for the device with the **SBP-TS-PSB** host.

Figure 8 shows external quantum efficiencies and power efficiencies (η_p) of the devices with the **SBP-TS-PSB** host. The device **A** using $[(piq)_2Ir(acac)]$ as a guest shows the best performance with a maximum η_{ext} of 14.6% and η_p of 10.3 lm W^{-1} at $1.5\ mA\ cm^{-2}$. The maximum η_{ext} and η_p of other devices are 13.5%, 7.8 lm W^{-1} (at $1.3\ mA\ cm^{-2}$) and 9.9%, 7.0 lm W^{-1} (at $0.5\ mA\ cm^{-2}$) for the devices **B** and **C**, respectively. Although the devices show a gradual decrease in efficiencies with increase in current as explained above, the EL efficiencies remain high at a practical brightness of $100\ cd\ m^{-2}$; 14.5% (7.1 lm W^{-1}), 13.4% (6.6 lm W^{-1}), and 9.8% (5.3 lm W^{-1}) for $(piq)_2Ir(acac)$, $(piq)_3Ir$, and $(btp)_2Ir(acac)$, respectively. The performance of all devices is summarized in Table 1. The efficiencies of devices **A**, **B**, and **C** using the **SBP-TS-PSB** host are significantly higher than those obtained with the common CBP host as shown in Figure 7 and previous reports using $(btp)_2Ir(acac)$ as a red phosphorescent emitter (~7%, ~4.6 lm W^{-1} at $J = 0.1\ mA\ cm^{-2}$).[2d]

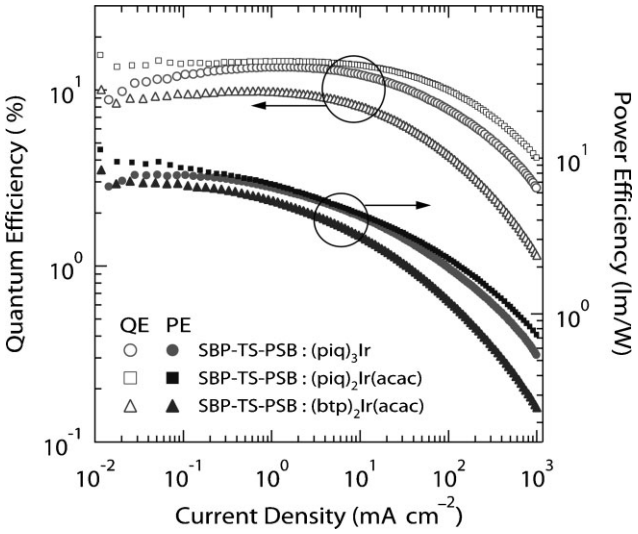

Figure 8. External quantum efficiencies (η_{ext}, open symbols) and power efficiency (η_p, closed symbols) as functions of current density for devices consisting of the **SBP-TS-PSB** host doped with $(piq)_3Ir$, $(piq)_2Ir(acac)$, and $(btp)_2Ir(acac)$.

3. Conclusions

We introduced a novel thermally and morphologically stable host material containing **SBP-TS-PSB** for red phosphorescent OLEDs. The molecular design of the host material helped achieve bipolar charge transport and proper HOMO, LUMO, and triplet energies suitable for the formation and confinement of excitons in the emitting layer. The electrophosphorescence devices based on the **SBP-TS-PSB** as a host and typical red-emitting phosphorescent iridium complexes as emitters exhibit high performances with very high external quantum efficiencies and power efficiencies compared with devices using the common CBP host. The external quantum efficiencies, power efficiency and Commission International de L'Eclairage color coordinates obtained from the $(piq)_2Ir(acac)$, $(piq)_3Ir$, and $(btp)_2Ir(acac)$-based devices are 14.6%, 10.3 lm W^{-1} (0.68, 0.32) at $J = 1.5\ mA\ cm^{-2}$, 13.5%, 7.8 lm W^{-1} (0.66, 0.32) at $J = 1.3\ mA\ cm^{-2}$, and 9.9%, 7.0 lm W^{-1} (0.66, 0.31) at $J = 0.5\ mA\ cm^{-2}$, respectively.

4. Experimental

SBP-TS-PSB was synthesized according to the procedures in Scheme 1. Unless stated otherwise, all reagents were used as received from commercial sources. The solvents were dried using standard procedures. All reactions were performed under purified nitrogen atmosphere using the standard Schlenk technique.

2-(9,9′-Spirobifluoren-2-yl)-4,4,5,5-Tetramethyl-1,3,2-Dioxaborolane (1): *n*-Butyllithium (8.70 ml, 13.92 mmol, 1,6 M solution in hexane) was added to a solution of 2-bromo-9,9′-spirobifluorene (5.00 g, 12.65 mmol) in dry THF (100 mL) at −78 °C. The mixture was stirred at room temperature for 3 h. After the reaction mixture was cooled to −78 °C. 2-Isopropoxy-4,4,5,5-tetramethyl-1,3,2-dioxaborolane (2.82 g, 15.16 mmol) was added to the reaction mixture. The solution was warmed slowly to room temperature and then stirred for 15 h. The reaction mixture was quenched with H_2O and extracted with Et_2O. The organic extracts were washed with brine and H_2O, and then dried over $MgSO_4$. After the solvent was evaporated, the crude product was purified by column chromatography (eluent = hexane/chloroform; 6:4 v/v), the product was recrystallized from chloroform/

methanol. Yield: 61% (3.41g). ^{1}H-NMR (300 MHz, CD_2Cl_2): δ 7.91–7.95 (m, 4H), 7.83–7.86 (dd, $J = 6.0$ Hz, 1H), 7.38–7.45 (m, 3H), 7.09–7.12 (m, 3H), 7.07–7.09 (s, 1H), 6.70–6.73 (m, 3H), 1.26 (s, 12H). ^{13}C-NMR (75 MHz, CD_2Cl_2): δ 149.93, 149.19, 148.55, 145.30, 142.49, 142.11, 135.06, 130.21, 128.96, 128.41, 124.40, 124.37, 121.16, 120.79, 120.13, 84.34, 25.84. LCMS-IT-TOF $[M+H]^+$: calcd. 443.2180; found: 443.2157.

1-Bromo-4-(9,9′-Spirobifluoren-2-yl)Benzene (2): 2-(9,9′-Spirobifluoren-2-yl)-4,4,5,5-tetramethyl-1,3,2-dioxaborolane (3.00 g, 6.78 mmol) and 1-bromo-4-iodobenzene (1.92 g, 6.78 mmol) were mixed in dry toluene. K_2CO_3 (2.0 M, 14 mL) was added, and the mixture was stirred. The mixture was degassed and tetrakis(triphenylphosphine)palladium (0.39 g, 0.34 mmol) was added in one portion under an atmosphere of N_2. The solution was then heated under reflux for 24 h under N_2. After the reaction mixture cooled, the solvent was evaporated and the product was extract chloroform. The organic extracts were washed with brine and H_2O, and then dried over $MgSO_4$. After the solvent was evaporated, the crude product was purified by column chromatography (eluent = hexane/chloroform, 8:2 v/v), the product was recrystallized from chloroform/methanol. Yield: 67% (2.14 g). ^{1}H-NMR (300 MHz, CD_2Cl_2): δ 7.88–7.96 (m, 4H), 7.60–7.63 (dd, $J = 6.0$ Hz, 1H), 7.36–7.45 (m, 5H), 7.28–7.31 (m, 2H), 7.10–7.15 (m, 3H), 6.91–6.92 (m, 1H), 6.68–6.75 (m, 3H). ^{13}C-NMR (75 MHz, CD_2Cl_2): δ 150.24, 149.74, 149.13, 142.43, 142.08, 141.81, 140.29, 140.09, 132.20, 129.12, 128.55, 128.43, 127.25, 124.40, 124.33, 122.73, 121.84, 121.11, 120.85, 120.73. LCMS-IT-TOF $[M]^+$: Calcd. 470.0670; found: 470.0653.

1-(9,9′-Spirobifluoren-2-yl)-4-(4,4,5,5-Tetramethyl-1,3,2-dioxaborolan-2-yl)Benzene (3): 1-Bromo-4-(9,9′-spirobifluoren-2-yl)benzene (2.00 g, 4.24 mmol), n-butyllithium (2.91 ml, 4.65 mmol, 1,6 M solution in hexane) and 2-isopropoxy-4,4,5,5-tetramethyl-1,3,2-dioxaborolane (0.95 g, 5.10 mmol) were allowed to react according to a procedure for compound 1. Yield: 55% (1.21 g). ^{1}H-NMR (300 MHz, CD_2Cl_2): δ 7.89–7.98 (m, 4H), 7.68–7.73 (m, 3H), 7.37–7.46 (m, 5H), 7.11–7.16 (m, 3H), 6.99–7.00 (m, 1H), 6.68–6.77 (m, 3H), 1.32 (s, 12H). ^{13}C-NMR (75 MHz, CD_2Cl_2): δ 150.10, 149.82, 149.21, 143.82, 142.45, 142.06, 141.90, 141.11, 135.54, 128.48, 128.43, 128.41, 127.54, 126.70, 124.43, 124.31, 122.98, 121.04, 120.84, 120.73, 84.34, 25.23. LCMS-IT-TOF $[M]^+$: calcd. 518.2414; found: 518.2409.

SBP-TS-PSB: Bis(3-bromophenyl)diphenylsilane (1.00 g, 2.02 mmol), 1-(9,9′-spirobifluoren-2-yl)-4-(4,4,5,5-tetramethyl-1,3,2-dioxaborolan-2-yl)benzene (2.31 g, 4.46 mmol), K_2CO_3 (2.0 M, 8 ml), and tetrakis(triphenylphosphine)palladium (0.24 g, 0.21 mmol) were allowed to react according to a procedure for compound 1. Yield: 57% (1.29 g). ^{1}H-NMR (300 MHz, CD_2Cl_2): δ 7.78–7.95 (m, 10H), 7.63–7.67 (m, 8H), 7.58–7.61 (m, 2H), 7.35–7.45 (m, 22H), 7.03–7.15 (m, 6H), 6.82–6.94 (m, 2H), 6.68–6.74 (m, 6H). ^{13}C-NMR (75 MHz, CD_2Cl_2): δ 149.58, 149.13, 148.64, 141.84, 141.39, 141.18, 140.17, 139.85, 139.62, 136.29, 135.34, 134.72, 133.88, 129.72, 128.33, 128.24, 127.94, 127.83, 127.22, 127.19, 126.64, 123.82, 123.73, 122.24, 120.43, 120.21, 120.12; LCMS-IT-TOF $[M+H]^+$: calcd. 1116.4230; found: 1116.4242. Anal. calcd. for $C_{86}H_{56}Si$: C, 92.44; H, 5.05%; found: C, 92.36; H, 5.06%.

Instrumentation: The ^{1}H and ^{13}C NMR spectra were recorded at 25 °C on a Bruker DPX-300 spectrometer. Mass spectra were recorded on a Shimadzu LCMS-IT-TOF. EA were recorded on a CE Instrument EA 1110 Elemental Analyzer. DSC was performed on a TA Instruments DSC 2020 instrument with a heating rate of 10 °C min^{-1} and a cooling rate of 20 °C min^{-1}. TGA was conducted on a TA Instruments TGA 2050 unit under a heating rate of 10 °C min^{-1} and a nitrogen flow rate of 90 mL min^{-1}. Cyclic voltammetry (CV) was carried out using an EG&G potentiostat/galvanostat model PARSTAT 2273 (Prinston Applied Research, USA). The reduction and oxidation potential measurements were carried out in anhydrous CH_2Cl_2 (for oxidation) or THF (for reduction) solution containing 0.5 mM SBP-TS-PSB and 0.1 M tetrabutylammonium hexafluorophosphate ($TBAPF_6$) as the electrolyte at room temperature in an argon environment. A platinum disk (diameter: 1.6 mm) and a platinum wire were used as working and counter electrodes, respectively. A platinum wire was used as the pseudo-reference electrode, and all the potential values were calibrated based on the ferrocene/ferrocenium (Fc/Fc^+) redox couple as an internal standard. UV/Vis spectra were measured with an HP 8453 spectrophotometer. Fluorescence spectra of **SBP-TS-PSB** solution and film were obtained at room temperature and phosphorescence spectrum of **SBP-TS-PSB** in a dilute 2-methyltetrahydrofuran solution was taken at 77 K using a Hitachi F-4500 fluorescence spectrometer.

Device Fabrication and Measurements: OLEDs were fabricated according to the following procedure: the ITO substrate with a sheet resistance of about 10 $\Omega\ \square^{-1}$ was cleaned ultrasonically in organic solvents (isopropyl alcohol, acetone, and methanol), rinsed in deionized (DI) water, and dried in an oven at 120 °C for more than 30 min. Prior to the deposition of organic layers, PEDOT:PSS was spin-coated (4000 rpm) with thickness of 40 nm on the UV ozone cleaned ITO substrate, and it was dried in a vacuum oven at 120 °C for more than an hour. Subsequently α-NPD, TCTA, **SBP-TS-PSB** doped with three phosphorescent guests of $(piq)_3Ir$, $(piq)_2Ir(acac)$, or $(btp)_2Ir(acac)$, BCP, Alq_3, LiF, and Al electrodes were successively deposited on the substrates, without breaking vacuum of about $2–3 \times 10^{-6}$ Torr. The deposition rate was about 1–2 Å s^{-1} for organic materials, and 4–5 Å s^{-1} for Al electrodes. The active area of the devices, defined by the overlap of ITO and Al cathode, was 1.96 mm^2. The current–voltage–luminance characteristics and the EL spectra were measured at room temperature using a Keithley 236 source-measure unit and a Keithley 2000 multimeter equipped with a photomultiplier tube (PMT) through an ARC 275 monochromator. The external quantum efficiency of the EL, defined as the ratio of the emitted photons to the injected electric charges, was calculated from the EL intensity measured by using a calibrated Si photodiode placed at an angle normal to the device's surface, assuming that the device was a Lambertian source.

Acknowledgements

This work was supported by the NANO Systems Institute–National Core Research Center (NSI-NCRC) from the Korea Science and Engineering Foundation (KOSEF) and the Brain Korea 21 Program endorsed by the Ministry of Education, Science and Technology of Korea. Supporting Information is available online from Wiley InterScience or from the author.

Received: September 5, 2008
Revised: October 13, 2008
Published online: January 12, 2009

[1] a) Eds: S. Miyata, S. H. S. Nalwa, *Organic Electroluminescent Materials and Devices*, Cordon and Breach, New York **1997**. b) C. H. Chen, J. Shi, C. W. Tang, *Macromol. Symp.* **1997**, *125*, 1. c) C. H. Chen, J. Shi, C. W. Tang, *Coord. Chem. Rev.* **1998**, *171*, 161. d) U. Mitschke, P. Bauerle, *J. Mater. Chem.* **2000**, *10*, 1471. e) L. S. Hung, C. H. Chen, *Mater. Sci. Eng, R.* **2002**, *39*, 143. f) C. W. Tang, S. A. Van Slyke, C. H. Chen, *J. Appl. Phys.* **1989**, *65*, 3610. g) J. Shi, C. W. Tang, *Appl. Phys. Lett.* **1997**, *70*, 1665. h) L. S. Hung, C. H. Chen, *Mater. Sci. Eng. R.* **2002**, *39*, 1665. i) C. W. Tang, S. A. Van Slyke, *Appl. Phys. Lett.* **1987**, *51*, 913.

[2] a) M. A. Baldo, S. Lamansky, P. E. Burrows, M. E. Thompson, S. R. Forrest, *Appl. Phys. Lett.* **1999**, *75*, 4. b) C. Adachi, M. A. Baldo, S. R. Forrest, M. E. Thompson, *Appl. Phys. Lett.* **2000**, *77*, 904. c) Y. Kawamura, S. Yanagida, S. R. Forrest, *J. Appl. Phys.* **2002**, *92*, 87. d) C. Adachi, M. A. Baldo, S. R. Forrest, S. Lamansky, M. E. Thompson, R. C. Kwong, *Appl. Phys. Lett.* **2001**, *78*, 1622. e) S. Lamansky, P. Djurovich, D. Murphy, F. Abdel-Razzaq, H.-E. Lee, C. Adachi, P. E. Burrows, S. R. Forrest, M. E. Yhompson, *J. Am. Chem. Soc.* **2001**, *123*, 4304. f) C. Adachi, R. Kwong, S. R. Forrest, *Org. Electron.* **2001**, *2*, 37. g) I. Tanaka, S. Tokito, in *Highly Efficient OLEDs with Phosphorescent Materials*, (Ed: H. Yersin), Wiley-VCH, Weinheim **2008**, Ch. 8.

[3] A. Tsuboyama, H. Iwawaki, M. Furugori, T. Mukaide, J. Kamatani, S. igawa, T. Moriyama, S. Miura, T. Takiguchi, S. Okada, M. Hoshino, K. Ueno, *J. Am. Chem. Soc.* **2003**, *125*, 12971.

[4] Y.-J. Su, H.-L. Huang, C.-L. Li, C.-H. Chien, Y.-T. Tao, P.-T. Chou, S. Datta, R.-S. Liu, *Adv. Mater.* **2003**, *15*, 884.

[5] a) C.-L. Li, Y.-J. Su, Y.-T. Tao, P.-T. Chou, C.-H. Chien, C.-C. Cheng, R.-S. Liu, *Adv. Funct. Mater.* **2005**, *15*, 387. b) F.-I. Wu, H.-J. Su, C.-F. Shu, L. Luo,

W.-G. Diau, C.-H. Cheng, J.-P. Duan, G.-H. Lee, *J. Mater. Chem.* **2005**, *15*, 1035. c) D. K. Rayabarapu, B. M. J. S. Paulose, J.-P. Duan, C.-H. Cheng, *Adv. Mater.* **2005**, *17*, 349. d) S. Okada, K. Okinaka, H. Iwawaki, M. Furugori, M. Hashimoto, T. Mukaide, J. Kamatani, S. Igawa, A. Tsuboyama, T. Takiguchi, K. Ueno, *Dalton Trans.* **2005**, 1583. e) T.-H. Kwon, H. S. Cho, M. K. Kim, J.-W. Kim, J.-J. Kim, K. H. Lee, S. J. Park, I.-S. Shin, H. Kim, D. M. Shin, Y. K. Chung, J.-I. Hong, *Organometallics* **2005**, *24*, 1578. f) F.-M. Hwang, H.-Y. Chen, P.-S. Chen, C.-S. Liu, Y. Chi, C.-F. Shu, F.-I. Wu, P.-T. Chou, S.-M. Peng, G.-H. Lee, *Inorg. Chem.* **2005**, *44*, 1344.

[6] a) K.-T. Wong, Y.-M. Chen, Y.-T. Lin, H.-C. Su, C.-C. Wu, *Org. Lett.* **2005**, *7*, 5361. b) P.-I. Shih, C.-L. Chiang, A. K. Dixit, C.-K. Chen, M.-C. Yuan, R.-Y. Lee, C.-T. Chen, E. W.-G. Diau, C.-F. Shu, *Org. Lett.* **2006**, *8*, 2799.

[7] K.-T. Wong, Y.-L. Liao, Y.-T. Lin, H.-C. Shu, C.-C. Wu, *Org. Lett.* **2005**, *7*, 5131.

[8] J. Pei, J. Ni, X.-H. Zhou, X.-Y. Cao, Y.-H. Lai, *J. Org. Chem.* **2002**, *67*, 4924.

[9] Y.-Y. Lyu, J. Kwak, O. Kwon, S.-H. Lee, D. Kim, C. H. Lee, K. Char, *Adv. Mater.* **2008**, *20*, 2720.

[10] A. D. Becke, *J. Chem. Phys.* **1993**, *98*, 5648.

[11] C. Lee, W. Yang, R. G. Parr, *Phys. Rev. B* **1988**, *37*, 785.

[12] M. J. Frisch, G. W. Trucks, H. B. Schlegel, G. E. Scuseria, M. A. Robb, J. R. Cheeseman, V. G. Zakrzewski, J. A. Montgomery, Jr., R. E. Stratmann, J. C. Burant, S. Dapprich, J. M. Millam, A. D. Daniels, K. N. Kudin, M. C. Strain, O. Farkas, J. Tomasi, V. Barone, M. Cossi, R. Cammi, B. Mennucci, C. Pomelli, C. Adamo, S. Clifford, J. Ochterski, G. A. Petersson, P. Y. Ayala, Q. Cui, K. Morokuma, D. K. Malick, A. D. Rabuck, K. Raghavachari, J. B. Foresman, J. Cioslowski, J. V. Ortiz, A. G. Baboul, B. B. Stefanov, G. Liu, A. Liashenko, P. Piskorz, I. Komaromi, R. Gomperts, R. L. Martin, D. J. Fox, T. Keith, M. A. Al-Laham, C. Y. Peng, A. Nanayakkara, C. Gonzalez, M. Challacombe, P. M. W. Gill, B. G. Johnson, W. Chen, M. W. Wong, J. L. Andres, M. Head-Gordon, E. S. Replogle, J. A. Pople, Gaussian 98 Revision A.9; Gaussian, Inc., Pittsburgh, PA **1998**.

[13] K. Brunner, A. van Dijken, H. Börner, J. J. A. M. Bastiaansen, N. M. M. Kiggen, B. M. W. Langeveld, *J. Am. Chem. Soc.* **2004**, *126*, 6035.

[14] I. Avilov, P. Marsal, J.-L. Bredas, D. Beljonne, *Adv. Mater.* **2004**, *16*, 1624.

[15] J. D. Anderson, E. M. McDonald, P. A. Lee, M. L. Anderson, E. L. Ritchie, H. K. Hall, T. Hopkins, E. A. Mash, J. Wang, A. Padias, S. Thayumanavan, S. Barlow, S. R. Marder, G. E. Jabbour, S. Shaheen, B. Kippelen, N. Peyghambarian, R. M. Wightman, N. R. Armstrong, *J. Am. Chem. Soc.* **1998**, *120*, 9646.

[16] B. D. Chin, C. H. Lee, *Adv. Mater.* **2007**, *19*, 2061.

[17] B. D. Chin, M. C. Suh, M. H. Kim, S. T. Lee, H. D. Kim, H. K. Chung, *Appl. Phys. Lett.* **2005**, *86*, 133505.

[18] N. Matsusue, S. Ikame, Y. Suzuki, H. Naito, *Appl. Phys. Lett.* **2004**, *85*, 4046.

[19] H.-I. Baek, C. H. Lee, *J. Appl. Phys.* **2008**, *103*, 054510.

[20] C. Adachi, M. A. Baldo, S. R. Forrest, *J. Appl. Phys.* **2000**, *87*, 8049.

[21] M. A. Baldo, C. Adachi, S. R. Forrest, *Phys. Rev. B* **2000**, *62*, 10967.

[22] S. Reineke, K. Walzer, K. Leo, *Phys. Rev. B* **2007**, *75*, 125328.